doi:10.26443/seismica.v4i1.1148

SEISMICA

Migration of Seismicity from the Mantle to the Upper Crust Beneath Harrat Lunayyir Volcanic Field, Saudi Arabia

Alexander R. Blanchette [1,2], **Simon L. Klemperer** [* 1], **Walter D. Mooney** [† 2], **Turki A. Sehli**[3]

[1]Stanford University, [2]United States Geological Survey, [3]Saudi Geological Survey

Author contributions: *Writing - Original draft*: Alexander R. Blanchette. *Visualization*: Alexander R. Blanchette. *Methodology*: Alexander R. Blanchette. *Investigation*: Alexander R. Blanchette. *Data curation*: Alexander R. Blanchette, Turki A. Sehli. *Formal Analysis*: Alexander R. Blanchette, Simon L. Klemperer, Walter D. Mooney. *Software*: Alexander R. Blanchette. *Supervision*: Simon L. Klemperer, Walter D. Mooney. *Conceptualization*: Simon L. Klemperer, Walter D. Mooney. *Writing - Review & Editing*: Simon L. Klemperer, Walter D. Mooney. *Funding acquisition*: Simon L. Klemperer, Walter D. Mooney. *Resources*: Turki A. Sehli.

Abstract Harrat Lunayyir is a volcanic field in Saudi Arabia that experienced a M_w 5.4 earthquake driven by an upper-crustal dike intrusion in May 2009. This volcanic field has exhibited numerous forms of volcanic seismicity both prior to and since the 2009 dike intrusion. Significantly, earthquakes within the lithospheric mantle and, rarely, the lower crust are present in the two-decade long seismicity catalog of Harrat Lunayyir. Here we analyze 24 years of volcanic seismicity at Harrat Lunayyir from 1998 to 2022. We find that: 1) precursory seismicity began at least eight years prior to the 2009 event, with a particularly notable seismic episode one year prior; 2) lithospheric mantle seismicity is highly localized in space and in time, largely occurring in discrete sequences lasting on the order of a few hours to a few days; 3) one seismic sequence clearly migrates upward from the lithospheric mantle to the upper crust, including seismicity within the nominally ductile lower crust; 4) crustal seismicity has been slowly declining over time; and 5) lithospheric-mantle seismicity does not show any apparent decline with time. From these observations we infer that the seismicity is driven by magmatic fluids or volatiles, and seismic monitoring of this volcanic field should continue into the future.

Production Editor:
Gareth Funning
Handling Editor:
Atalay Ayele Wondem
Copy & Layout Editor:
Hannah F. Mark

Received:
November 3, 2023
Accepted:
February 1, 2025
Published:
February 27, 2025

1 Introduction

Earthquakes within the lower crust and the lithospheric mantle are rare and therefore of scientific interest (Chen and Molnar, 1983; Molnar, 2020). We distinguish between two general types of seismic activity within these regions: 1) tectonic earthquakes and 2) volcanic earthquakes. We discuss each of these in turn.

1.1 Deep Tectonic Seismicity

Tectonic (non-volcanic) earthquakes within the continental lower crust and lithospheric mantle are rare and attract scientific attention when well recorded. Some of these deep earthquakes occur near the Moho, leading to a debate whether they have occurred in the lower crust or the lithospheric mantle. The very existence of lower-crustal earthquakes is controversial because the lower crust is often assumed to be ductile (Chen and Molnar, 1983; Molnar, 2020). Prominent examples are deep-crustal and upper-mantle earthquakes recorded beneath the Tibetan plateau, a region of active tectonics (Monsalve et al., 2009; Schulte-Pelkum et al., 2019; Song and Klemperer, 2024; Wang and Klemperer, 2021).

Some earthquakes within the lithospheric mantle have occurred in nominally inactive environments, such as the M_w 4.8 Wyoming intra-plate earthquake of 21 September 2013, hypothesized to have occurred within a localized region of concentrated slip at a mid-lithospheric discontinuity or a brittle instability within a compositional heterogeneity (Prieto et al., 2017). Deep earthquakes also occur in volcanic settings, and it is the origin of these that is the focus of our paper.

1.2 Deep Volcanic Seismicity

Volcanoes and volcanic seismicity are widely studied due to their ability to profoundly impact humanity (Chouet, 2003; Chouet and Matoza, 2013). Of particular note, White and McCausland (2019) developed a model of volcano seismicity that is not simply empirical but built upon inferred volcanic processes from a multitude of multidisciplinary observations from around the world. The model of White and McCausland (2019), based upon 36 volcanic/seismic episodes at 26 volcanoes–predominantly island-arc and continental-arc volcanoes–is separated into four distinct stages of pre-eruptive volcanic seismicity:

Stage One: The first stage of volcanic seismic activity is driven by magmatic intrusions within the lower crust—typically at depths of 10 to 40 km, though it can reach deeper. The energy radiated from this seismicity is dominantly low-frequency and usually devoid of high

*sklemp@stanford.edu
†mooneyusgs@gmail.com

frequencies. However, this low-frequency energy may go unobserved due to limitations of local short-period seismographic networks.

Stage Two: Commonly, the first volcanic seismicity observed is second-stage volcanic seismicity. It is composed of volcano-tectonic (VT) seismicity of likely tectonic (brittle-failure) origin triggered by volcanic activity. These events occur in the upper crust, near the location of the eventual eruption, if an eruption occurs. VT seismicity that occurs farther away (2–30 km) is called distal VT seismicity.

Stage Three: As the eruption draws nearer, seismicity associated with volcanic vent-clearing becomes evident. It is tied to the shallow upper crust (<3 km) and is characterized by low-frequency earthquakes and seismic tremor.

Stage Four: In the fourth and final stage, shallow, repetitive seismicity/harmonic tremor coincides with the final ascent of magma.

As we show in this paper, Harrat Lunayyir (Fig. 1) provides examples of the first two stages, in particular demonstrating seismicity not only in the lower crust but also in the lithospheric mantle (Blanchette et al., 2018; Blanchette, 2022) (Fig. 2), as also documented elsewhere (Molnar, 2020).

1.3 Harrat Lunayyir Geologic Background

The Arabian shield is the eastern portion of the Arabian-Nubian shield (ANS) that formed by amalgamation of numerous terranes along suture zones, including the Yanbu suture beneath Harrat Lunayyir (Johnson et al., 2013; Stern and Johnson, 2010). Roughly 500 Myr after its formation, the ANS rifted apart both due to far-field plate forces and the impingement of the Afar Plume at ~30 Ma. This rifting separated Arabia from the ANS by the Red Sea plate boundary, which extends from the Afar Triple Junction to the Dead Sea Transform (Fig. 1). The Arabian plate has experienced two distinct phases of volcanism. During the first phase (30–20 Ma), contemporaneous with Afar plume impingement at the base of the lithosphere (Stern and Johnson, 2010), tholeiitic-to-transitional lavas were emplaced along rift-parallel dikes extending the entire length of the Red Sea rift flank. The lithosphere was significantly thinned prior to the second phase (12 Ma to present) (Blanchette et al., 2018) in which transitional-to-strongly alkalic lavas were erupted forming the younger harrats (basaltic volcanic fields), including Harrat Lunayyir (Fig. 1).

A dike intruded into the upper crust beneath Harrat Lunayyir during April through June 2009 in a magmatic-tectonic event. During this event there were >30,000 earthquakes, culminating in a M_w 5.4 earthquake and an 8-km long surface rupture (Pallister et al., 2010). We refer to the M_w 5.4 event and its aftershocks as the Harrat Lunayyir volcano-tectonic crisis. Interferometric synthetic aperture radar (InSAR) data imply that this sequence occurred during the intrusion of a 0.13 km^3 dike

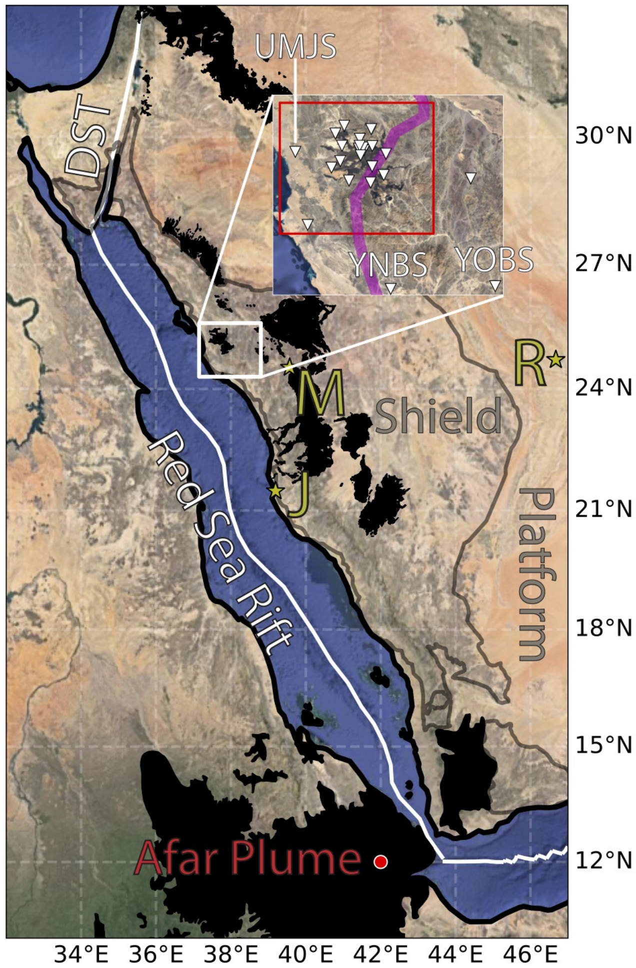

Figure 1 DST–Dead Sea Transform, M—Medinah, J—Jeddah, R—Riyadh. Black marks Cenozoic volcanic fields (on all maps). **Inset** (white box) shows Harrat Lunayyir seismic array, with stations operational prior to the 2009 intrusion labelled. Magenta line in the inset, and following maps, is the Yanbu Suture (Johnson et al., 2013). Red box denotes bounds of Fig. 2.

that reached from ~12 km depth to within 1 km of the surface with maximum dike opening of ~4 m, equivalent to a strain of $\sim 10^{-3}$ (Pallister et al., 2010). It is not uncommon for a dike to come close to the surface without erupting (Gudmundsson, 1990). In this case, the failure to erupt was perhaps due to a shallow layer of rigid basalt (Koulakov et al., 2015) that effectively blocked the final ascent. Following the M_w 5.4 mainshock, the local seismic array was greatly expanded to monitor Harrat Lunayyir and provide early warning of a potential volcanic eruption. Since this near-eruption, Harrat Lunayyir has continued to be seismically active, especially around the shallow dike intrusion, and seismicity has not decayed following Omori's Law as expected for tectonic aftershock sequences.

Harrat Lunayyir has a crustal thickness of 34±2 km (Blanchette et al., 2023a,c) and a lithospheric thickness of 60.0±5.0 km (Blanchette et al., 2018). Relocation of lithospheric-mantle earthquakes for 2014, the only year for which we have waveform data, show them aligned along a plane striking N103°E and dipping toward N193°E (Blanchette et al., 2018). Earthquake geothermometry combined with local surface heat flow shows that the lithosphere beneath Harrat Lunayyir reached its present thickness 12±2 Ma and has not yet achieved thermal equilibrium with the asthenosphere beneath it (Blanchette et al., 2018).

We find that prior to the 2009 volcanic crisis, there were multiple similar, smaller episodes of increased seismic activity beneath Harrat Lunayyir, with a particularly active episode approximately one year before the crisis. Seismicity peaked during the 2009 crisis and has since been weakly decaying over time. Once the array achieved sufficient seismographic station density, in mid-2010 (post-crisis), it began routinely detecting earthquakes within the lithospheric mantle.

In this paper, we review the seismicity of Harrat Lunayyir. We first discuss the seismic catalog prior to the volcanic crisis, then the activity during the crisis. Finally, we look at the seismicity that continues for over a decade beyond the crisis (Tab. S1). We categorize pre- and syn-crisis seismicity only by depth. We can analyze post-crisis seismicity by spatial patterns as well as depth, due to improved seismograph coverage, using Bayesian-Gaussian Mixture Modelling (BGMM). For the post-crisis analysis, we also apply a seismic-sequence detection algorithm to study the temporal pattern of seismicity and moment release to gain insight into the evolution of Harrat Lunayyir over the 24-year-long seismic catalog.

2 Data and Methods

2.1 Seismic Dataset

We used the earthquake catalog from the Saudi Geological Survey (SGS) that begins on 16 September 1998 and ends on 31 May 2022 (Fig. 2 and Tab. S1). Earthquake locations and magnitudes were determined with Atlas software (Nanometrics) and a regional seismic velocity model. All post-2009 events were located using arrival times at three or more seismic stations. The number of seismic stations available for locating earthquakes versus time is indicated in Fig. 2b. The seismic network can locate events greater than $\mathrm{M_l}$ 1.5, and the catalog is complete for events over $\mathrm{M_l}$ 3.5.

2.1.1 Spatial Categorization of Seismicity

In our analysis of the seismic catalog, we separate the earthquakes into different spatial categories. However, earthquakes prior to mid-2010 are less well-located due to significantly fewer stations, and smaller events are more likely to be missed. When discussing the older portions of the catalog, or the entire catalog, we can only bin the events into very general depth categories (upper crust, lower crust, and mantle lithosphere). More recent portions of the seismic catalog are significantly better constrained due to the denser network, which allowed us to detect finer-scale spatial and temporal patterns of the earthquakes. Due to the amount of data in the catalog (>50,000 earthquakes), manual categorization would be non-trivial. Hence, we employed three different methods of automatic categorization common in data science (k-means, Gaussian Mixture Modelling, and BGMM). The results of all three methods are quite similar, so we built our analysis from BGMM, the most general of the three methods. Our analysis would not change significantly if we had chosen one of the other two methods instead.

BGMM (Roberts et al., 1998), as implemented in the scikit-learn Python library (Pedregosa et al., 2011), was employed to separate the post-crisis (better-located) catalog into five categories of seismicity from July 2010 to January 2018: (1) dike, (2) lower crust, (3) mantle, (4) distal VT, and (5) distal magmatic (Fig. 3). BGMM categorizes data points using a generalized form of Cartesian distance, by calculating a mixture of Gaussians that fit the data in a Bayesian framework. Both a limitation and a strength of BGMM is the lack of any *a priori* constraints on the categorical separation of events, and we imposed no categories prior to analysis.

Although we did not enforce a set number of categories for the BGMM algorithm (an important distinction from k-means analysis), we did initiate it with six categories. Upon completion of BGMM, the different groups were analyzed manually. Of note, in the raw results, the dike was split into three separate categories (deep, mid-depth, and shallow), and the deep category also included the spatially distinct lower-crustal events. We manually split the lower-crust earthquakes into a distinct category and merged the three dike categories into one. While some events are likely to be incorrectly categorized, we assume that the number of errors is low with respect to the total number of events (55,639) in the catalog. The Gaussians overlap in space, and for this reason, we cannot retroactively apply our BGMM categorization to the pre-crisis and syn-crisis seismicity (1998–2010). When studying the full catalog (1998–2022), we therefore revert to a simple separation into depth categories.

2.1.2 Magnitudes and Moments

The seismic catalog contains local magnitudes ($\mathrm{M_l}$) for each event (Deichmann, 2006; Ross et al., 2016). Due to the small magnitudes, saturation is not an issue. We calculated the frequency-magnitude distribution for each type of event (distal VT, distal magmatic, dike, lower crust, mantle lithosphere) assuming a standard Gutenberg-Richter log-linear relation (Eq. 1, Fig. 4):

$$log_{10}\left(N_{M\geq m}\right) = a - bM \tag{1}$$

We also plot a transformed version of the Gutenberg-Richter relation, where we have rotated the plots such that a value of b = 1.0 is a flat horizontal line to aid with visualization (Eq. 2, Fig. 4):

$$log_{10}\left(N_{M\geq m}\right) + M = a - (b-1)\,M \tag{2}$$

We calculated the moment release ($\mathrm{M_0}$, in N–m), assuming that local magnitude and moment magnitude ($\mathrm{M_w}$) are the same for earthquakes in the catalog, for each category and depth, and before and after the main diking event (Fig. 4). We used the standard relationship (Eq. 3; Hanks and Kanamori, 1979):

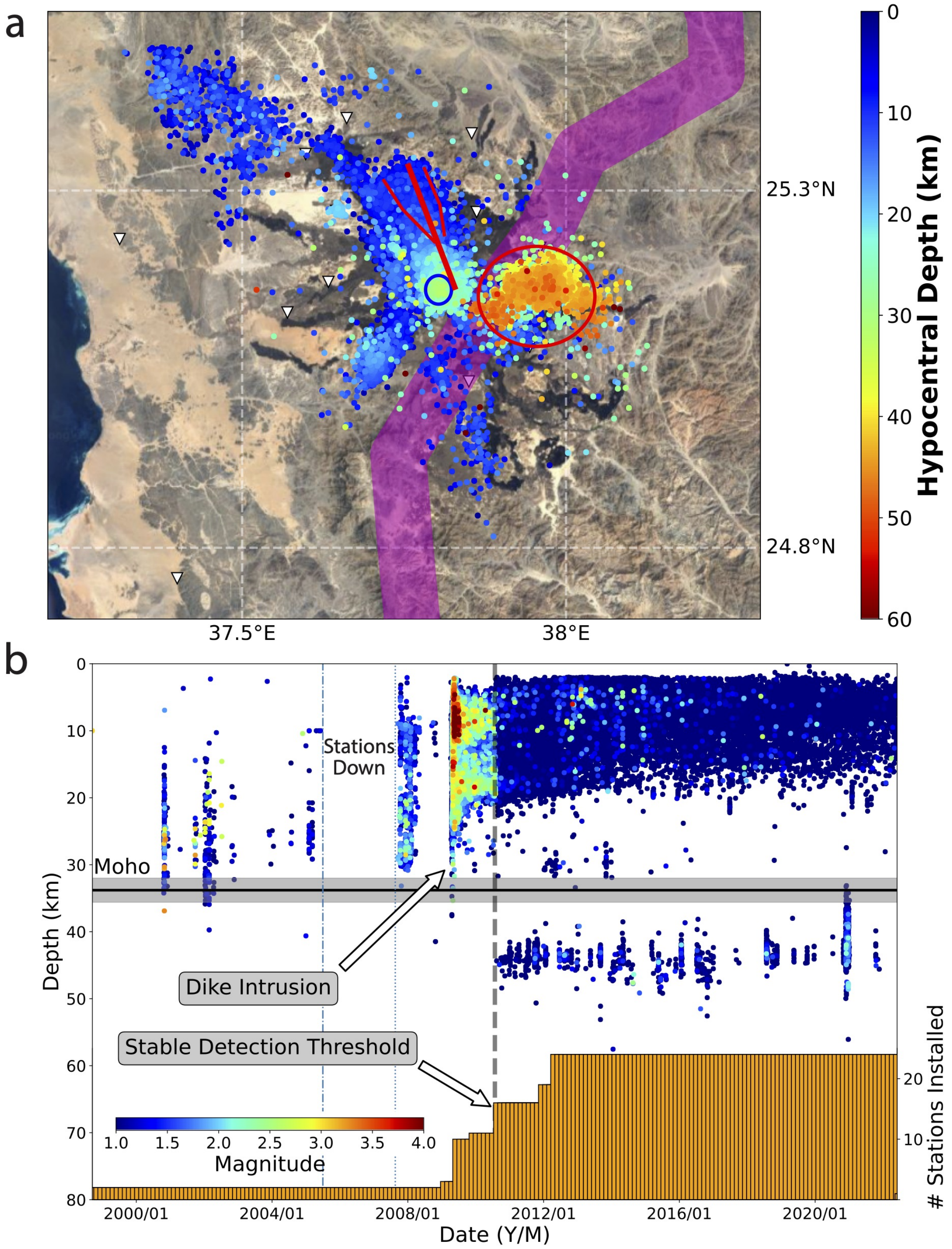

Figure 2 Complete Harrat Lunayyir seismic catalog, 1998–2022. a) Map view, color-coded by event depth. Red lines are the surface projection of the 2009 intrusion and the two graben-bounding normal faults from Pallister et al. (2010). Fiducial blue ellipse is approximate location of lower-crustal earthquakes post-July 2010. Fiducial red ellipse bounds the majority of mantle earthquakes. b) Depth-time plot of Harrat Lunayyir seismicity, color-coded by event magnitude. Larger magnitude earthquakes are plotted on top of smaller magnitude earthquakes. Orange histogram is number of stations installed.

$$M_0 = 10^{\frac{3}{2}\mathrm{M_w}+9.1} \tag{3}$$

2.1.3 Tectonic Seismicity

One possible hypothesis to explain the crustal seismicity is that the dike intrusion was essentially a slow extensional earthquake and that the earthquakes within the upper crust since then are merely aftershocks of this episode. This phenomenon would be modeled via Omori's Law (Eq. 4; Ōmori, 1894; Utsu, 1961):

$$R(t) = \frac{A}{(t+t_0)^p} \tag{4}$$

where R is the earthquake rate, A is a parameter for scaling aftershock activity, t is time elapsed, t_0 is a time offset constant to prevent singularity, and p is a constant exponent that is typically $\sim$1.

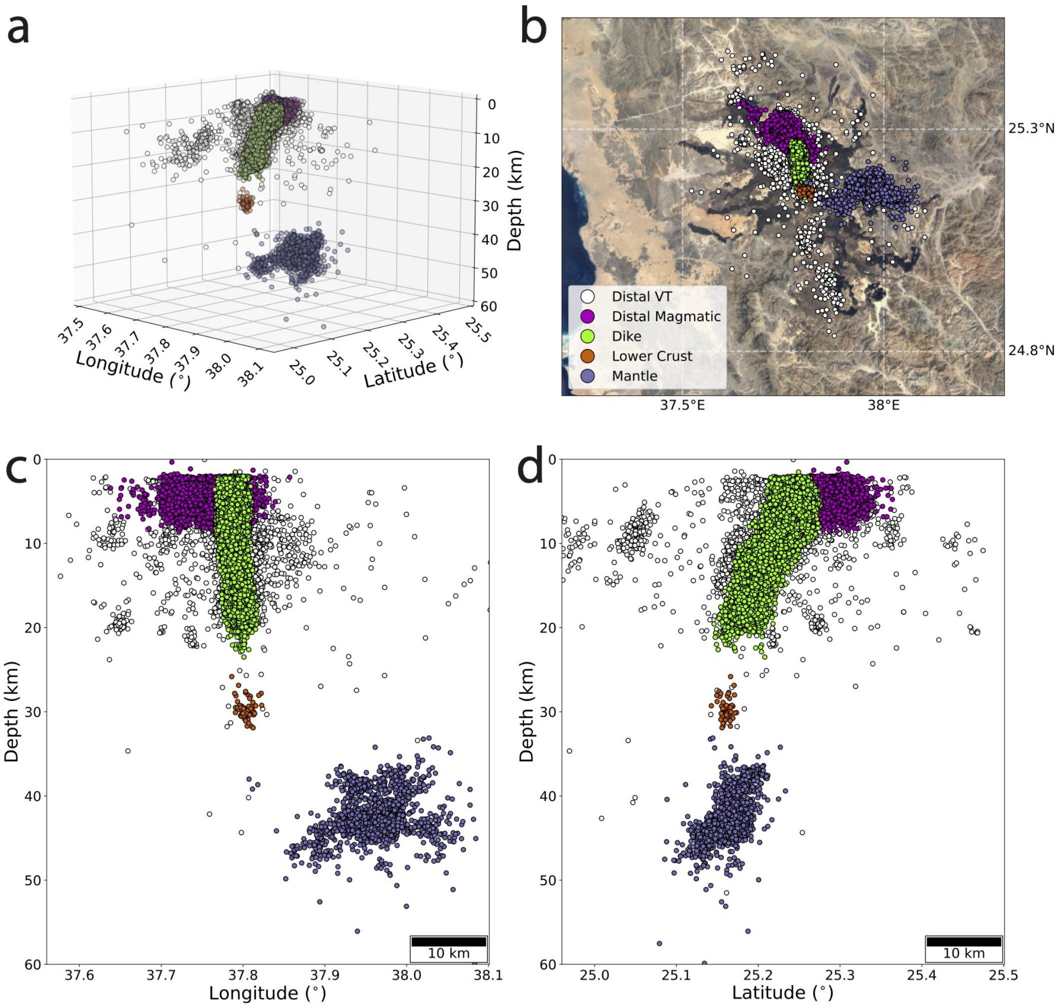

Figure 3 Post-intrusion catalog seismicity distributions from July 2010 to May 2022. a) Isometric view of earthquake seismicity, color-coded by category, b) Map view of seismicity, c) W–E cross-section, d) S–N cross-section. Moho depth is 34 km.

2.1.4 Seismic Sequences

We define an earthquake "sequence" using a histogram-based approach if (1) there are $\geq$ 3 earthquakes in 12 hours, and (2) temporal gaps in seismicity are < 5 days. We implemented this by first calculating the number of earthquakes within 12-hour temporal bins to generate a list of potential sequences. In the second processing step, consecutive potential sequences (i.e., neighboring 12-hour bins with $\geq$ 3 earthquakes) are joined. Finally, potential sequences that are separated in time by gaps of < 5 days are joined to create the final set of sequences (Tab. S2).

3 Results

We describe the seismic activity in chronological order: pre-crisis, syn-crisis, and post-crisis. The seismographic network around/within Harrat Lunayyir was expanded dramatically over the course of the recorded seismic catalog, thus the more recent data are more reliable. Seismic waveform data from 2014 allowed the relocation of mantle earthquakes using the program Hypoinverse (Klein, 2002), with the average absolute change in location of mantle earthquakes being $\sim$4 km to the west (maximum location change was < 9 km) (Blanchette et al., 2018). The relative change of earthquake location within the mantle cluster was $\leq$ 2 km. Mantle earthquakes are the least-well located due to their low magnitudes and the relatively small azimuthal coverage from the local array. Meanwhile, earthquakes in the lower crust and around the dike are better constrained as they are much closer to the array and have better overall azimuthal coverage. In summary, the certainty of any particular earthquake location increases with proximity to the array, both in terms of time (most recent is better constrained) and distance from the Earth's surface (nearer to the surface is better constrained).

3.1 Pre-Intrusion Seismicity

A three-station seismic array near Harrat Lunayyir began recording on 18 May 1998 (Tab. S1, Fig. 1). The first earthquake near Harrat Lunayyir was detected on 16 September 1998; it was small (M_l = 3.1) and shallow (10 km), and no further earthquake was detected until October 2000. From then until 2008, pulses of seis-

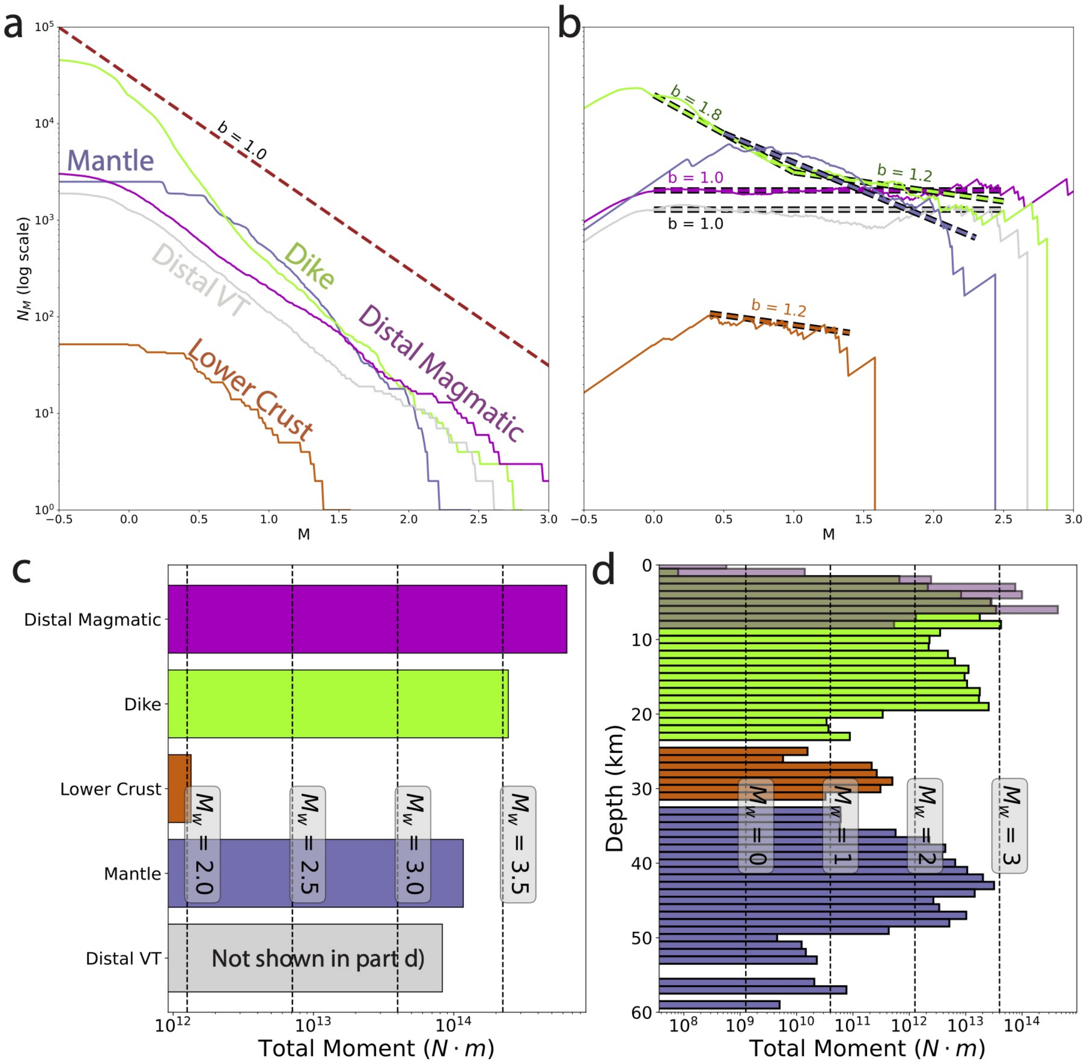

Figure 4 Magnitude and moment distributions. **Top** Magnitude-frequency plot of Harrat Lunayyir seismicity from July 2010 to January 2018. a) Standard Gutenberg-Richter plot, color-coded by earthquake category. b) Transformed G-R plot, such that b = 1 is a flat line. **Bottom** Seismic moment release from July 2010 to January 2018. c) Cumulative moment release for each category. d) Histogram of moment release for each category (except distal VT) against depth.

micity, reaching from the Moho to within 2 km of the surface, were repeatedly recorded beneath Harrat Lunayyir (Fig. 5b). The hypocentral parameters are not as well constrained as those after stabilization of the local array (post-2010); however, the epicenters of these earthquakes are collocated with the post-2010 mantle events (Fig. 5a). We take this collocation as evidence that the older reported locations are (at least) within a few kilometers of their true locations. The magnitude of the earthquakes recorded at Harrat Lunayyir during the 2000–2008 timeframe was $0.0 \leq M_l \leq 3.5$. The seismicity from 2000 through 2008 is highly localized in space, dominantly located in a small (~30-km diameter) cluster just southeast of the southernmost portion of the 2009 dike intrusion (Fig. 5). The seismicity extends from near the Moho (34±2 km depth), likely both above and below the Moho, to the shallow upper crust, in bursts of activity (~one week from start to finish) separated by gaps of up to a few years (e.g., March 2002–February 2005 in Fig. 5b). The apparent seismic quiescence from July 2005 to August 2007 (Fig. 5b) is due to there being no local array during that time (Tab. S1).

The local array began recording again on 19 August 2007, shortly after which multiple discrete episodes of seismicity ($1.0 \leq M_l \leq 3.0$) were recorded. This final, pre-crisis burst of seismicity is focused vertically above the post-crisis mantle earthquakes (Fig. 5) and was not associated with any detectable surface deformation (Xu et al., 2016). The seismicity again paused for approximately one year before the well-known volcanic crisis of 2009.

3.2 Seismicity during the 2009 near-eruption

Despite the bursts of seismicity in 2007 and earlier (Fig. 2), and the proximity to the nearby town of Al-Ays, which was evacuated in 2009, no additional seismic monitoring stations were installed until the United States Geological Survey (USGS) Volcano Disaster Assistance Program (VDAP) team arrived to help assess the situation in 2009 (Pallister et al., 2010).

Here, we discuss the seismicity of the volcanic crisis itself, beginning on 19 April 2009 and continuing through 25 July 2010, an end date chosen to mark the

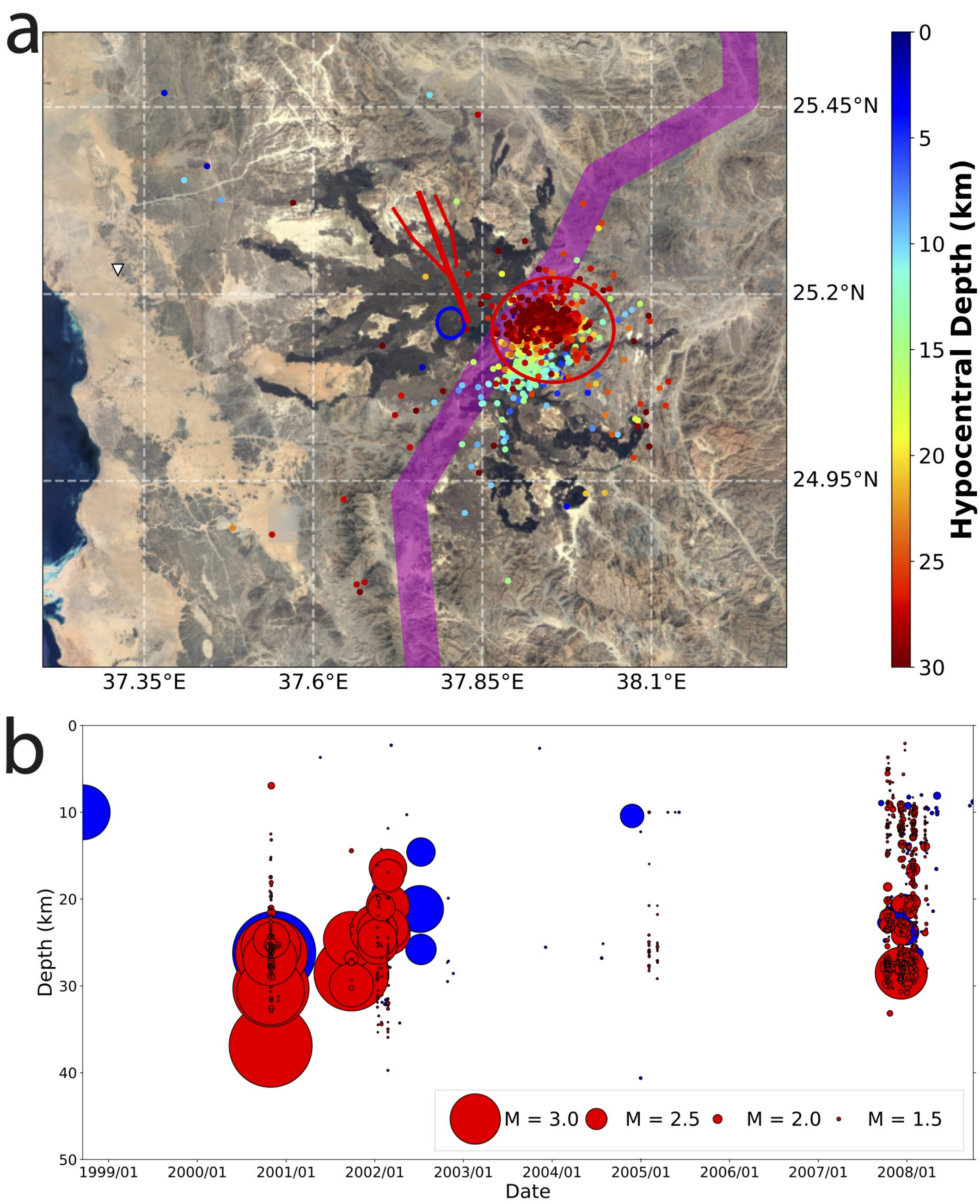

Figure 5 Pre-intrusion seismic history. a) Map of epicentral locations. White triangle is closest active seismic station (Fig. 1). 2009 dike and graben bounding normal faults (red lines) from Pallister et al. (2010). Yanbu suture (thick magenta line) from Johnson et al. (2013). Blue ellipse is location of post-intrusion lower-crustal seismicity. Red ellipse is location of post-intrusion mantle earthquakes. b) Depth-versus-time plot of pre-intrusion seismicity (no local stations were active from 07/2005 to 08/2007). Red circles are in sequences, blue are not in sequences. Circles scaled to seismic moment.

achievement of a stable earthquake-detection threshold as the Harrat Lunayyir seismic array neared completion and close to the end of InSAR-detectable ground deformation. The sudden start of seismicity marked the end of a 200-day period with zero nearby earthquakes recorded. At the start of the volcano-seismic crisis, the earthquake locations initially exhibited a bimodal depth distribution around 12 km and 23 km depth (Fig. 6). The seismic zone at 12 km depth started off with two distinct bursts of activity (20 April and 23 April 2009) (Fig. 6; Fig. S1), located south of the eventual dike intrusion. The more temporally continuous, deeper zone of seismicity activity was located in the lower crust directly above the location of the 1998–2008 seismicity and the mantle earthquakes recorded from 2010 onward (Fig. 6a).

Nine days after the start of the crisis, on 28 April 2009, both loci of seismicity beneath Harrat Lunayyir shallowed. This upward sweep of seismic activity was contemporaneous with an overall increase in seismicity, both the number of earthquakes and magnitude of earthquakes (Fig. 6b). A few days later, on 1 May 2009, there was a pulse of seismic activity originating from near-Moho depths (M 2.1 at 34 km depth) to 5 km beneath the surface (Fig. 6b). The loci of seismic activity temporarily stabilized at depths of ~5 km and ~15 km

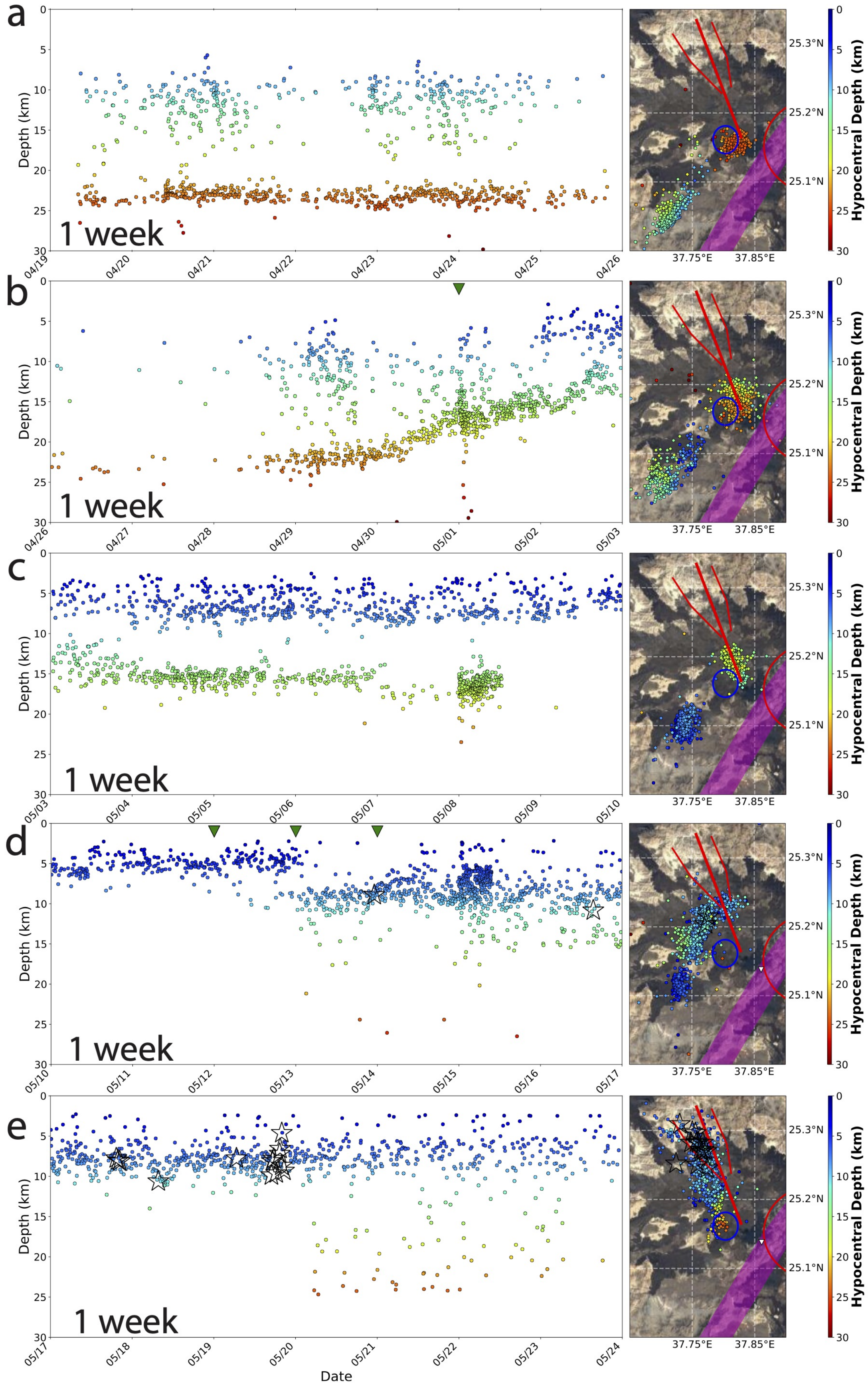

Figure 6 Weekly plots of seismicity during the 2009 intrusion episode. a) 19 April–26 April 2009. b) 26 April 2009–3 May 2009. c) 3 May 2009–10 May 2009. d) 10 May 2009–17 May 2009. e) 17 May 2009–24 May 2009. **Left** Inverted green triangles mark the installation of a new seismographic station. **Right** Inverted white triangles are currently active seismographic stations. Stars are earthquakes with magnitudes ≥ 4.

depth through 7 May 2009 (Fig. 6c). On 8 May 2009, there was a burst of small-magnitude earthquakes at ∼15 km, after which the deeper band of seismicity disappeared (Fig. 6c). There was no contemporaneous change in array geometry to explain this change in the seismicity. The shallower seismicity continued, with increasing magnitudes, and the southern and northern groups of seismicity joined (Fig. 6d). After 13 May 2009, the southern seismicity turned off, and the earthquakes began to migrate to the location of the final dike intrusion (Fig. 6d, Fig. S1), and $M \leq 4$ earthquakes began to occur, always in the region of the dike intrusion. Beginning on 20 May 2009, seismicity at depths of ∼20 km depth began to again nucleate at the same location as future lower-crustal earthquakes (Fig. 6e).

During the intrusion, the seismicity initially occurred in two areally separated clusters of activity (Figs. 6a,b,c), roughly aligned with the Yanbu suture (Gahlan et al., 2020; Johnson et al., 2013) (Fig. S1). On the 25th day of the intrusion seismicity, the bimodal seismicity merged into a single location that swept northward, first east of the eventual dike intrusion and then progressively propagated along the entirety of the dike. On day 31, the largest earthquakes occurred, and after that, the seismicity remained fairly constant through time for over a year, largely confined to and illuminating the entirety of the dike (Fig. 7). The few exceptions are earthquakes slightly to the west of the intrusion, at the location of the inferred upper-crustal magmatic storage reservoir (Koulakov et al., 2014). Over time, the seismicity rate decreased. We suggest that the relative paucity of lower-crustal and mantle seismicity prior to August 2010 was due to the local seismic array not being sufficiently dense to detect low-magnitude events at this depth and that the locations of pre-dike intrusion events are less well constrained due to the limited number of seismic stations (just three) within ∼100 km of Harrat Lunayyir (Fig. 1 inset).

3.3 Post-Intrusion Seismicity

3.3.1 Mantle Seismicity

Mantle earthquakes began to be detected beneath Harrat Lunayyir in July 2010 at depths of 40–50 km below the Earth's surface (Fig. 2b). These events are all in a very small region between latitudes 25.08–25.20°N and longitudes 37.85–38.10°E (Fig. 8), with a mean depth of ∼43 km (median and mode are also ∼43 km). The mantle seismicity occurs in discrete pulses that typically have durations of less than a few days, with weeks to months of quiescence between each sequence (Figs. 8 and 9). The events are not randomly located but occur along a plane that dips ∼45° south (Blanchette et al., 2018) with different pulses in slightly different locations (Fig. 10).

Because earthquakes within the lithospheric mantle occur episodically (Fig. 8), we used a histogram-based approach to group distinct mantle sequences in time (Fig. 9). We divided the time frame of well-recorded mantle seismicity (July 2010–May 2022) into 12-hour-long, non-overlapping bins (altering the start times of the bins does not affect our results). We selected all bins with at least three earthquakes as a "possible sequence" (Fig. 9a). Consecutive bins were merged to form longer, single sequences. There were 12 sets of resultant sequences that had time gaps of less than five days between them, which we manually merged.

The resultant 24 sequences (Tab. S2) capture ∼46% of the earthquakes within the lithospheric mantle. However, we miss the two largest earthquakes (Fig. 9b) because we did not use magnitude or seismic moment in the determination of mantle sequences, only earthquake rate. The two largest earthquakes occur during periods of relative BGMM quiescence; these and many of the larger events not in sequences lie in the deeper part of the depth distribution. To show that our sequences (Fig. 9) are not random groups of unrelated earthquakes, we plot each sequence in map view (Fig. 10). The mantle sequences occur in small, well-defined regions (Fig. 10), despite their definition only being based upon time. Hence, we presume that the sequences represent linked events.

Most sequences do not exhibit obvious depth migration patterns (Fig. 11), perhaps in part due to ∼1 km uncertainties in the depth of individual events, though we cannot rule out such behavior (Blanchette, 2022). Some sequences are clearly composed of smaller episodes, separated by less than a couple of days. Sequences 22 and 23 are the most seismically productive, lasting the longest (7–15 days) and composed of numerous subsequences (Fig. 12).

3.3.2 Lower Crust

The lower crust beneath Harrat Lunayyir has very few episodes of seismicity. It is the least active depth range beneath Harrat Lunayyir, both in terms of the number of earthquakes and the amount of seismic moment released. The combined seismic moment release in the lower crust from 2010 to 2018 is $\sim 10^{12}$ N–m, equivalent to a single M_w = 2.0 earthquake (Fig. 4c). The range of magnitudes within the lower crust is ∼0.3–1.4, with a b-value of 1.2, though the number of events and the limited magnitude range are both too small for any certainty that the b-value is sufficiently elevated to be reliably inferred to represent fluid-driven processes (Wiemer and McNutt, 1997). Lower-crustal seismicity is dominantly confined to two sequences: from January to June 2012 and from January to March 2014, and for the remaining 90% of that time range, it is sparse and follows no apparent pattern (Fig. 8b).

3.3.3 Upper Crust

The main post-intrusion dike seismicity detected by the Harrat Lunayyir array is, as shown from our mixture modelling, confined to a small region near the initial dike intrusion (Fig. 3a). Some distal VT seismicity, as characterized by BGMM, appears to form a halo around the dike and may more correctly be deemed dike seismicity, though we lack waveform data to make a more careful distinction. Other distal VT seismicity that is farther from the dike appears to occur in two local regions of weakness: one south of the intrusion striking ∼NNW–SSE and approximately collinear with the dike,

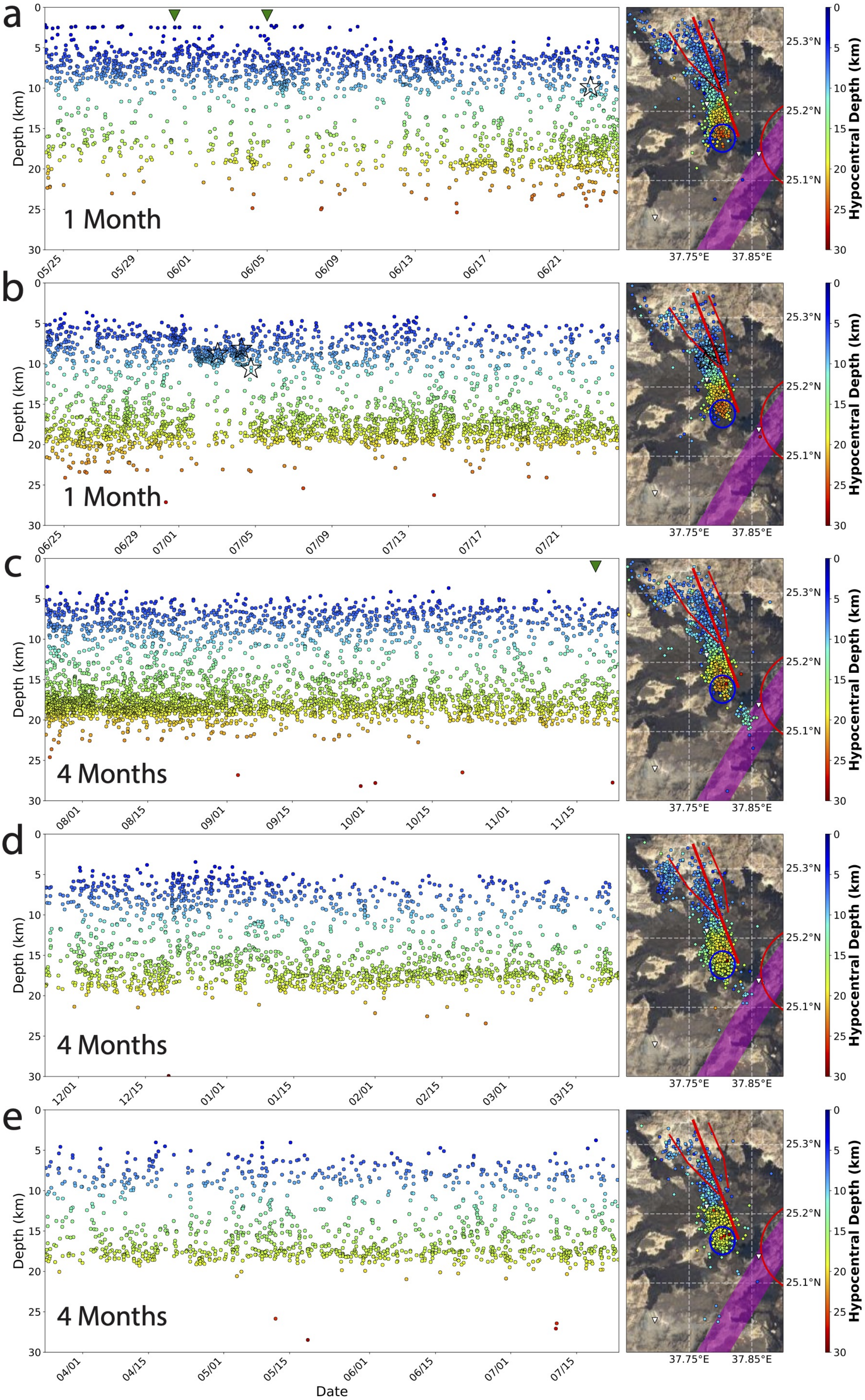

Figure 7 Evolution of Harrat Lunayyir seismicity in the months following the 2009 intrusion, for the period immediately following Fig. 6. a) 24 May 2009–24 June 2009. b) 24 June 2009–24 July 2009. c) 24 July 2009–24 November 2009. d) 24 November 2009–24 March 2010. e) 24 March 2010–24 July 2010.

and one northwest of the intrusion striking ~NW–SE. The distal VT seismicity since August 2010 has a total seismic moment release of $\sim 10^{14}$ N–m, or approximately that of a single M 3.3 earthquake (Fig. 4c). Our

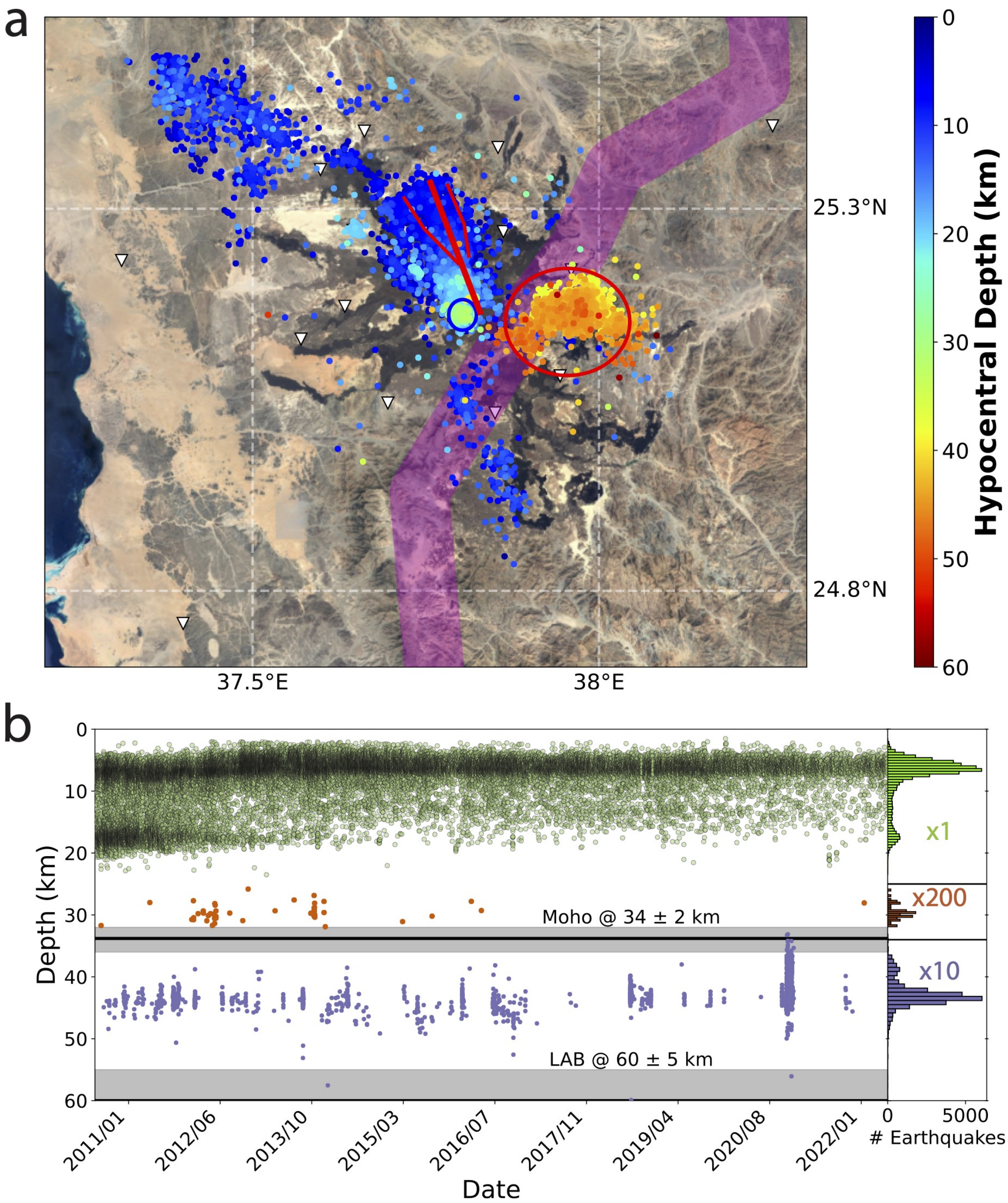

Figure 8 Post-dike-intrusion seismicity. a) Map view including all seismic categories. Symbols as in Figs. 2 and 3. b) Depth-time plot of catalog events, color-coded by category, excluding distal VT and distal magmatic events, with a depth histogram of earthquakes. LAB is the lithosphere-asthenosphere boundary (Blanchette et al., 2018).

distal VT category of seismicity has a Gutenberg-Richter b-value of ∼1 (Fig. 4b), supporting our interpretation that distal VT seismicity is standard tectonic seismicity (Wiemer and McNutt, 1997) triggered by the nearby intrusion.

Dike seismicity occurs continuously from the surface to 25-km depth with a bimodal depth distribution having two dominant peaks, at 7 km and at 18 km (Fig. 8b). The dike seismicity dominates the catalog, with an estimated moment release of $\sim 2 \times 10^{14}$ N–m since August 2010, the equivalent of nearly a M_w 3.5 earthquake during that time (Fig. 4c). For low magnitudes (0.0–1.0), the b-value is ∼1.8, while for larger magnitudes (1.0–2.5), the b-value is ∼1.2 (Fig. 4b), but this change does not appear correlated with depth. Recent dike intrusions in Iceland (Bárðarbunga) show seismicity marking magma flow that is at the base of the dike (Woods et al., 2019), in contrast to our post-crisis seismicity at Harrat Lunayyir, which encompasses all depths along the dike. The distal magmatic seismicity, which encompasses the largest amount of seismic moment release in the post-intrusion catalog, includes a shallow magma chamber centered at a depth of ∼5 km that was inferred from tomographic imaging (Koulakov et al., 2014) using data recorded from 30 April 2009–31 July 2009 (i.e., during the crisis).

3.4 Seismicity Decay Rates

We compared the seismic catalog against predictions from Omori's law (Ōmori, 1894; Utsu, 1961). The initial seismicity after the 2009 dike intrusion at a depth of

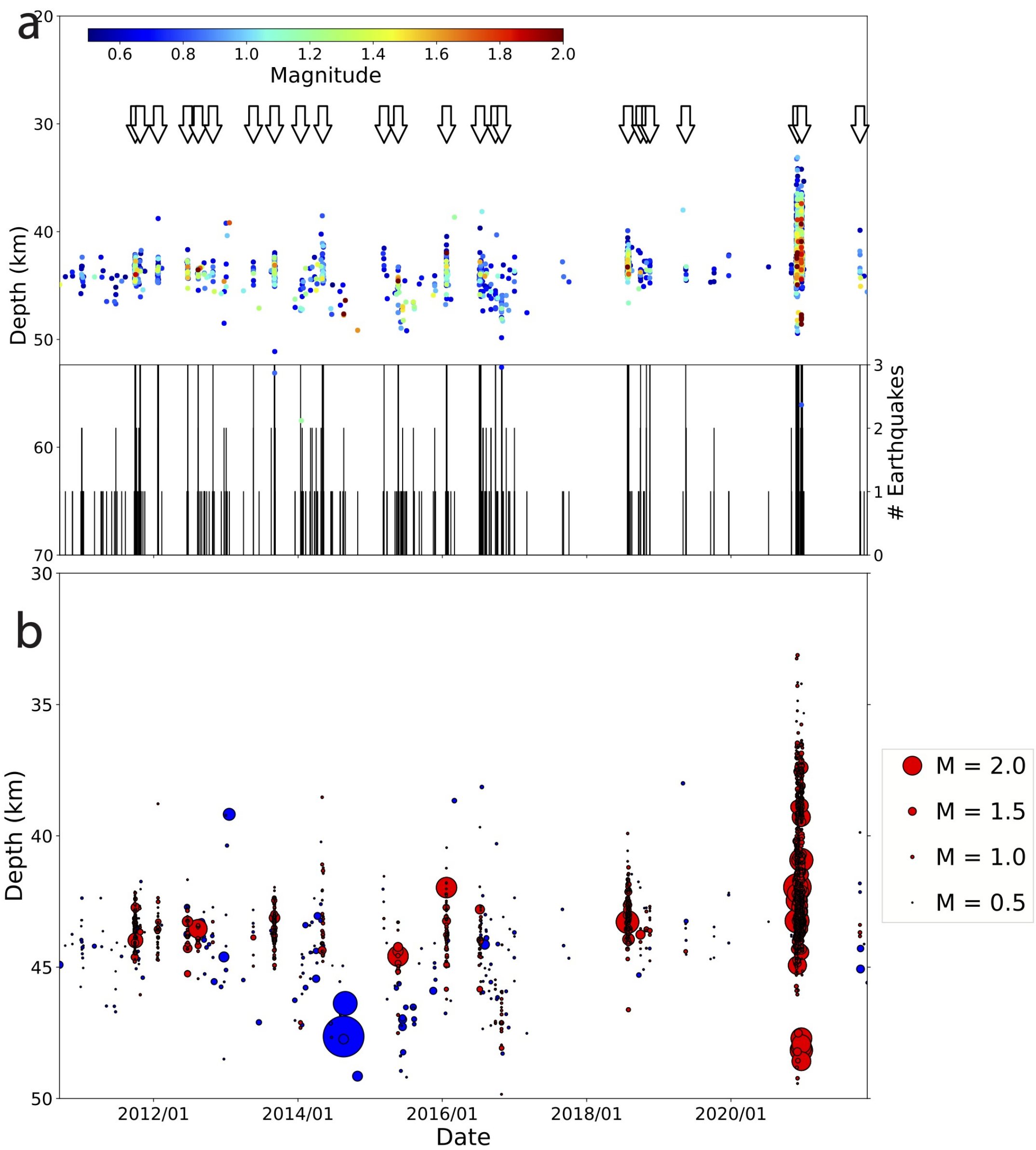

Figure 9 Sequence-detection results for post-crisis near- and below-Moho seismicity, plotted against date. a) Earthquake depths color-coded by magnitude (left axis) above a histogram (vertical lines) of daily earthquakes (right axis). The histogram is truncated to our cut-off of three earthquakes to make it easier to recognize sequences. White arrows are centered in time on the detected sequences. b) Mantle earthquake depths color-coded as red: part of a sequence, and blue: not in a sequence. Circles are scaled to earthquake moment.

0–15 km, through July 2010, can be modeled as an aftershock sequence (Fig. 13). This interpretation, however, is not possible for the earthquakes within the lower crust (25–34 km) and the lithospheric mantle (34–60 km, Fig. 13). The rate of earthquakes within the mantle is indicative of multiple discrete pulses of seismicity followed by periods of inactivity (Fig. 13b), not a continuous decay of seismicity back to distal volcano-tectonic levels. After July 2010, the rate of seismicity experiences a slight increase (Fig. 13), possibly due to array completion, and then in the shallow depth range maintains a slow temporal decay. In contrast, the 15–25 km deep seismicity drops off dramatically in a manner inconsistent with a single Omori curve.

3.5 Magmatically Driven Seismicity

We assume the 2009 dike intrusion was associated with the M 5.4 earthquake (Pallister et al., 2010). InSAR observations and modeling of ground deformation provide a volume of 1.3×10^8 m^3 in a dike with a surface area of ~ 64 km^2 and an average opening of ∼2 m (Pallister et al., 2010). Assuming the dike-intrusion centroid was at a depth of 5 km (spanning from 1 to 9 km), we expect the dike to have cooled and solidified in ∼10 days. Comparing dike volume from geodesy to seismic moment, the aseismic moment release during the diking episode within the cold and brittle upper crust (< 15 km) was ∼75–93% (Pallister et al., 2010) or ∼86% (Baer and Hamiel, 2010) of the total moment release. That is, most of the moment released was aseismic.

Earthquakes within the lithospheric mantle are likely

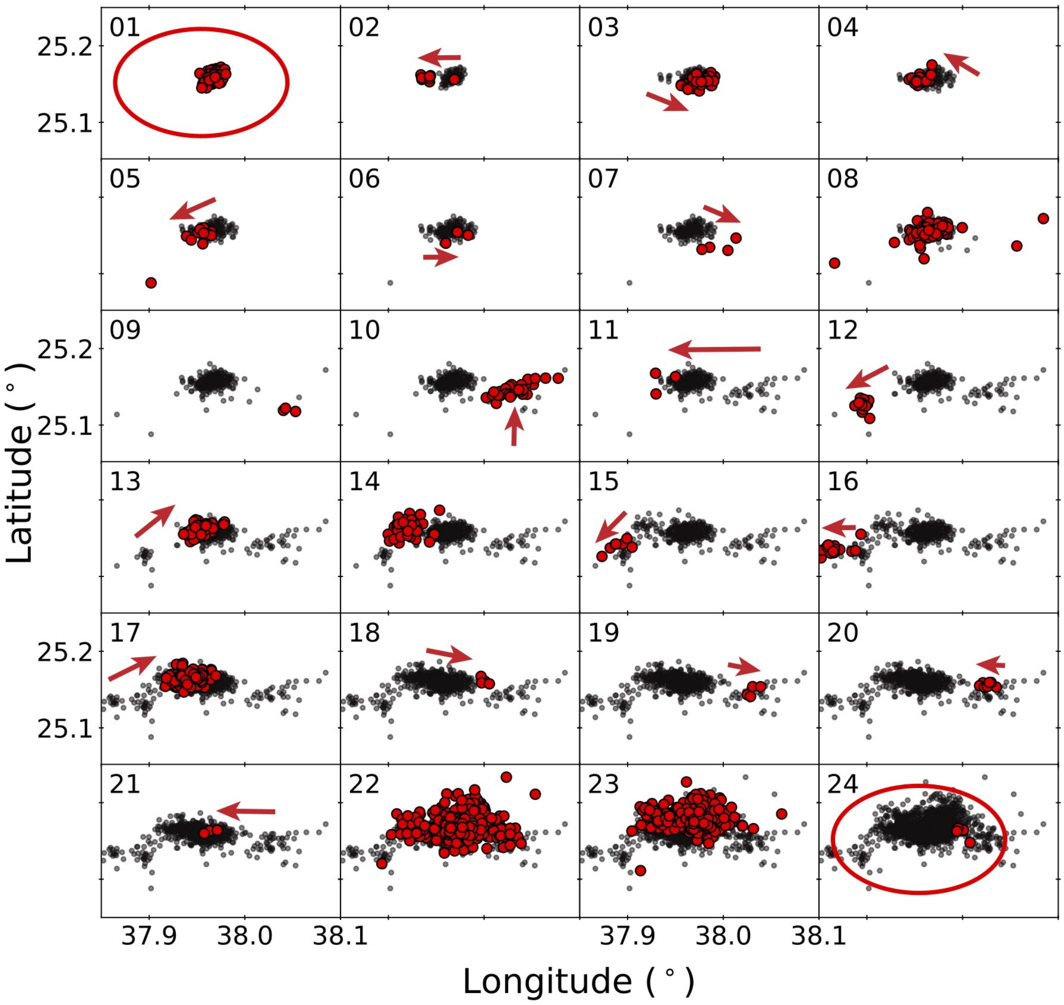

Figure 10 Map view plots of discrete mantle sequences. Red circles are the current sequence. Black circles are the past sequences. Red arrows are visual guides to show the approximate change in location between successive sequences. Estimated relative uncertainty (from the 2014 events) is roughly 4 km. Red ellipse is as in Fig. 2.

occurring just above the mantle brittle-ductile transition (Blanchette et al., 2018). These near-Moho earthquakes never achieve magnitudes larger than ~2.5 (with the exception of the earliest recorded, in 2000, Fig. 5b), and the lithospheric mantle is also significantly less seismogenic than the shallow crust (Fig. 8b). Our observations suggest that a significantly larger proportion of energy released in the lithospheric mantle is dissipated aseismically when compared with the upper crust. Although empirical estimates of magma volumes from seismic moment have been made for upper-crustal intrusions (White and McCausland, 2019), extrapolation to the lower crust or upper mantle is quite uncertain (Blanchette, 2022).

4 Discussion

The dike beneath Harrat Lunayyir was relatively small, 0.13 km^3 (Pallister et al., 2010), and should have frozen and become seismically quiet within only a few weeks to months of emplacement (Blanchette, 2022). Yet, it remained the most seismically active region within Saudi Arabia, even >10 years post-emplacement. The dike intrusion is nearly parallel to the Red Sea rift axis, suggesting that its orientation was likely tectonically controlled, or at least was stress-controlled since $\mathrm{SH}_{\max}$ is likely parallel to the rift. We hypothesize that seismicity may still be driven by magmatic fluids (such as CO_2 or melt) originating from mantle depths, as evidenced by the elevated b-value (Fig. 4), the close association between mantle earthquakes and the Yanbu suture, and the lower-crustal earthquakes along the suture, extending to the dike itself. Seismicity illuminates the dike from the surface to a depth of ~20 km (Fig. 8), approximately at the crustal brittle-ductile transition (Blanchette et al., 2018), and is directly above the much rarer lower-crustal events (Fig. 8).

The pre-dike seismicity seemed to try to find a vertical path through the crust, but failed until it migrated ~10 km laterally, breaking into the middle crust during the main diking episode (Figs. 5 and 6). It appears to have broken through along a SW–NE trending ophiolite within the Yanbu suture zone (Gahlan et al., 2020). The mantle seismicity is episodic, occurring in short bursts, but is far more common than the lower-crustal seismicity. The correlation between the location of mantle seismicity and pre-intrusion seismicity likely reflects focusing of melt migration from an as-

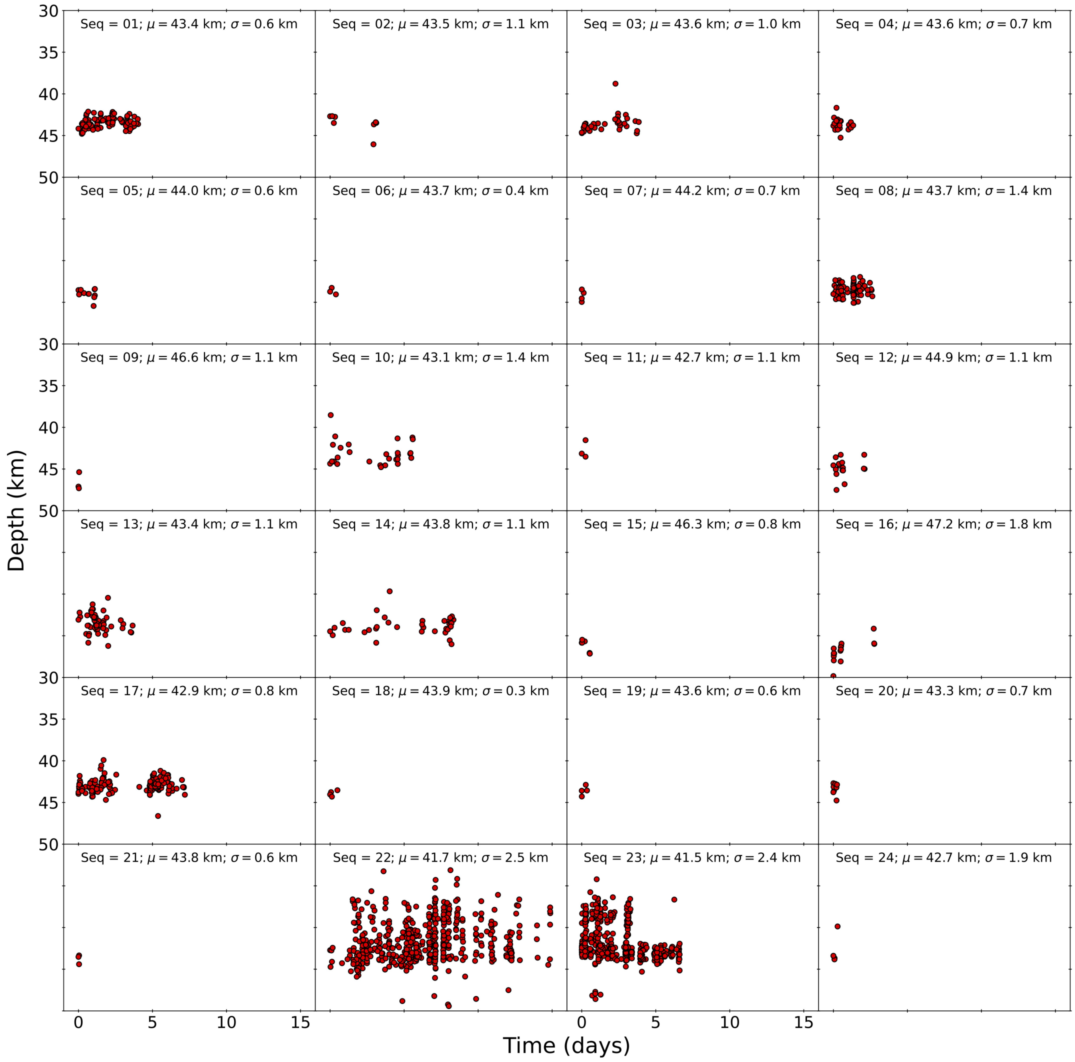

Figure 11 Depth plot of earthquake sequences versus time relative to sequence initiation. μ: average depth in sequence. σ: standard deviation of event depths in each sequence.

thenospheric source. The change in location of crustal seismicity correlates well with the location of the Yanbu suture zone, which likely represents a zone of weakness (possibly due to compositional heterogeneities). We cannot determine whether magma passes through the lower crust both seismically and aseismically (percolating upwards along grain boundaries), or whether frequent magma pulses from the mantle via localized subvertical channels pool near the Moho and only occasionally rise upward seismically. Seismicity within the lithosphere may occur via a fault-fracture mesh (Hill, 1977), with a mixture of opening cracks and slip on normal/reverse faults linking cracks.

Repeated dike intrusions in the lithospheric mantle provide a mechanism by which melt could accumulate below the base of the crust, but the accumulated volumes beneath Harrat Lunayyir are insufficient to underplate the crust by observable amounts, neither elevating the Vp/Vs ratio nor increasing crustal thickness (Blanchette et al., 2023a; Tang et al., 2016) beyond those of the surrounding area. Instead, the intrusion must remain molten long enough to accumulate sufficient melt to buoyantly force its way past the gravitational stalling depth (~40 km) and through the lower crust. Even less frequently, melt later intrudes into the upper crust at the deepest extent of the seismicity related to the dike, such as the apparent sequence near the end of 2013 (Fig. 8). Similar vertically migrating seismicity has been observed elsewhere and interpreted as due to upward migration from depth of magmatic fluids (either volatiles or melt) (e.g., Mammoth Mountain, Hotovec-Ellis et al. (2018); Iceland, Ágústsdóttir et al. (2016)), though perhaps nowhere else so clearly from the upper mantle through the lower crust to the upper crust.

Harrat Lunayyir remains the most seismically active region within Saudi Arabia. Well-documented transcrustal migration sequences continued to occur at least through 2022. This is demonstrated both in the raw number of earthquakes and in the seismic moment release (Fig. 13). The seismicity beneath Harrat Lunayyir continues to occur at three main depths: 1) upper crust, 2) mid-to-lower crust, and 3) within the mantle lithosphere, implying that there has been no appreciable depletion of the asthenospheric magma source. We recommend that monitoring continue in the region, as we have no means of knowing whether diking or even eruption will occur within the next decade(s).

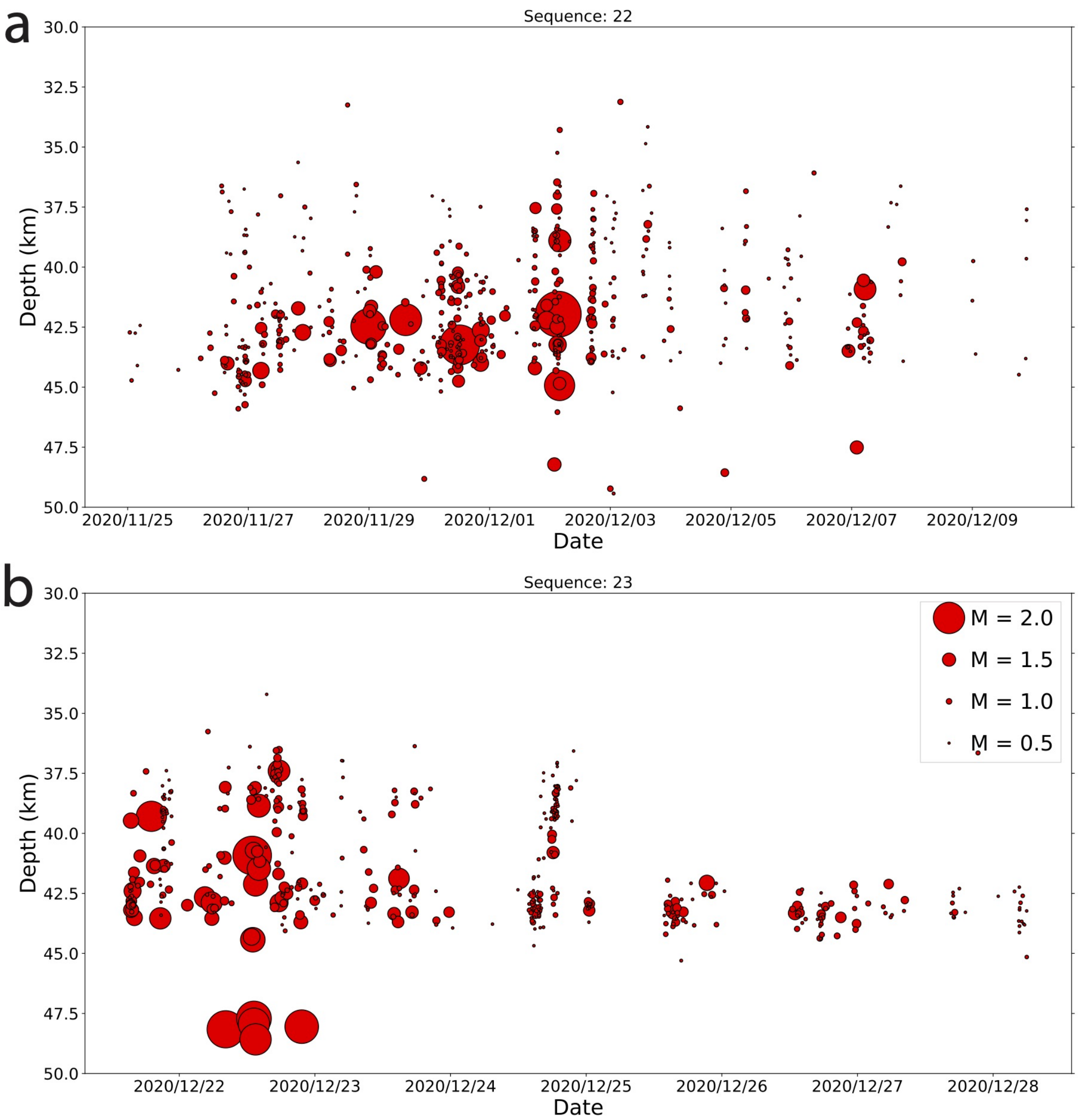

Figure 12 Evolution of earthquake depths in sequences 22 and 23. a) Sequence 22. b) Sequence 23.

5 Conclusion

The seismic catalog beneath Harrat Lunayyir provides insights into the evolution of a young volcanic field adjacent to the Red Sea rift. We have analyzed the patterns of seismicity within the catalog against time, space, and earthquake magnitude. Our analysis leads to the following conclusions regarding the seismicity beneath Harrat Lunayyir:

1) Mantle seismicity is likely driven by magma, or possibly volatiles, sourced from the asthenosphere.

2) Mantle seismicity appears to be confined to a localized conduit or narrow planar zone and does not have the same orientation as the shallow dike.

3) Much of the shallow (0–15 km depth) seismicity in Harrat Lunayyir can be considered as aftershocks of the 2009 dike intrusion, in contrast with the mantle seismicity which occurs in discrete episodes.

4) Lower-crustal seismicity is limited, and the lower crust probably deforms aseismically when the flux-rate of magmatic fluids is too low to generate detectable seismicity.

5) Vertical propagation of magmatic fluids can be tracked from seismicity.

6) Greater spatial coverage of seismic monitoring in the region following the first trans-crustal migration of seismicity in 2001 could have increased awareness of the potential for a volcanic crisis and strong earthquake.

7) Had such monitoring been available, however, no specific prediction could have been made, as the crisis occurred following months of relative seismic quiescence, and most clear lower-lithosphere seismic sequences have not been followed by volcano-tectonic crises.

Acknowledgements

The authors thank P. Segall, E. Van Dyke, D. Shelly, J. Hardebeck, L. Namazie, and two anonymous reviewers for their helpful comments that greatly improved this manuscript.

Data and code availability

The seismic data used in this study were recorded by the Saudi National Seismic Network, operated by

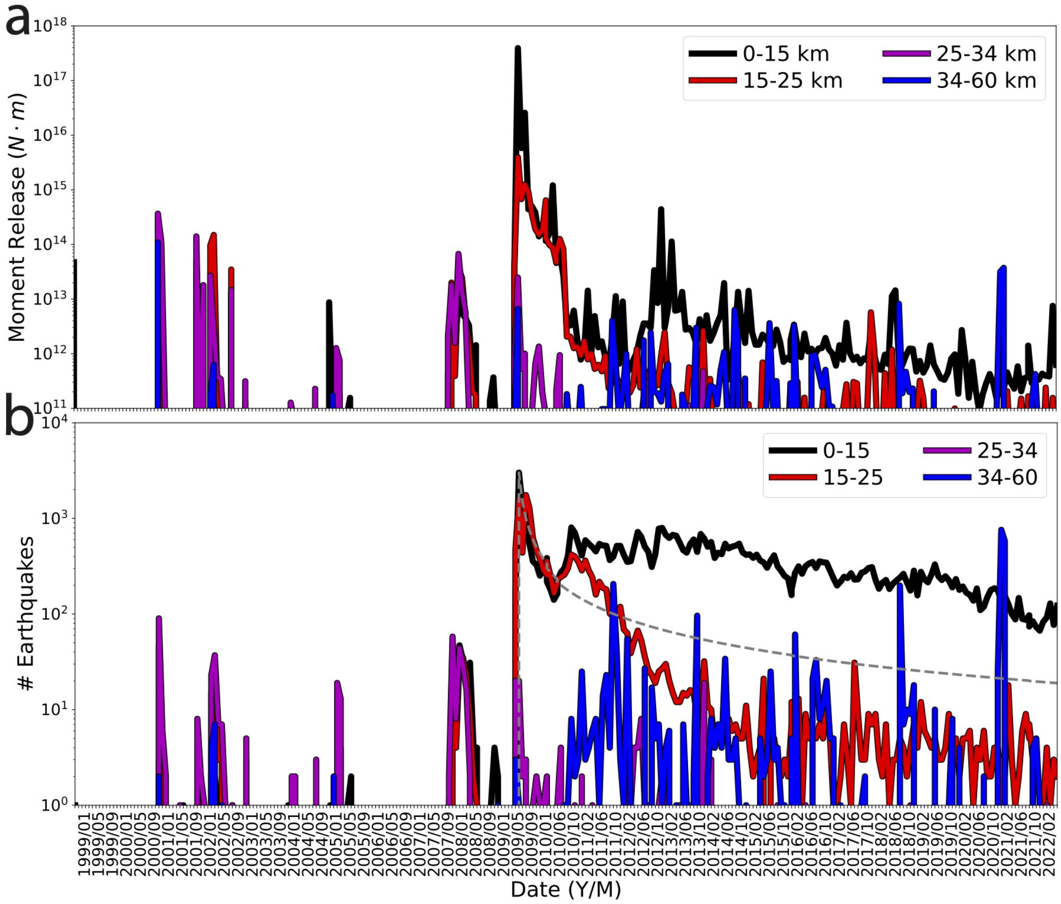

Figure 13 Monthly seismic rate for the entire earthquake catalog. a) Expressed as moment release. b) Expressed as the number of earthquakes. Divisions are made on depth so as to include the full catalog (1999–2022). Dash gray curve is an Omori law fit to the peak seismicity in the 0–15 km depth range with an exponent of 1.0.

the Saudi Geological Survey (SGS). The seismic data used may be requested from the SGS (https://sgs.gov.sa/en/e-services). Analysis codes are available online (Blanchette et al., 2023b). Any use of trade, firm, or product names is for description purposes only and does not constitute an endorsement by Stanford University or the United States Geological Survey.

Competing Interests

The authors do not have any competing interests.

References

Ágústsdóttir, T., Woods, J., Greenfield, T., Green, R. G., White, R. S., Winder, T., Brandsdóttir, B., Steinthórsson, S., and Soosalu, H. Strike-slip faulting during the 2014 Bárðarbunga-Holuhraun dike intrusion, central Iceland. *Geophysical Research Letters*, 43 (4):1495–1503, 2016. doi: 10.1002/2015GL067423.

Baer, G. and Hamiel, Y. Form and growth of an embryonic continental rift: InSAR observations and modelling of the 2009 western Arabia rifting episode. *Geophysical Journal International*, 182(1):155–167, 2010. doi: 10.1111/j.1365-246X.2010.04627.x.

Blanchette, A. R. *Structural Seismology of the Arabian Plate and Volcano Seismology Near the Red Sea Rift Margin*. PhD thesis, Stanford University, 2022. https://purl.stanford.edu/cf318hv6989. ProQuest Dissertations and Theses, 29755973.

Blanchette, A. R., Klemperer, S. L., Mooney, W. D., and Zahran, H. M. Two-stage Red Sea rifting inferred from mantle earthquakes in Neoproterozoic lithosphere. *Earth and Planetary Science Letters*, 497:92–101, 2018. doi: 10.1016/j.epsl.2018.05.048.

Blanchette, A. R., Klemperer, S. L., and Mooney, W. D. Crustal thickness and the Vp/Vs ratio within the Arabia Plate from P-wave receiver functions at 154 broadband seismic stations. Open-file Report 2023-1042, US Geological Survey, 2023a. doi: 10.3133/ofr20231042.

Blanchette, A. R., Klemperer, S. L., and Mooney, W. D. Analysis and modeling codes - Decadal seismicity and dike freezing - Harrat Lunayyir, Saudi Arabia, 2023b. doi: 10.5281/zenodo.10119526.

Blanchette, A. R., Klemperer, S. L., Mooney, W. D., and Zahran, H. M. Thickness of the Saudi Arabian Crust. In Sisson, T. W., Calvert, A. T., and Mooney, W. D., editors, *Active volcanism on the Arabian Shield-Geology, volcanology, and geophysics of northern Harrat Rahat and vicinity, Kingdom of Saudi Arabia: U.S. Geological Survey Professional Paper 1862*, chapter M. 2023c. doi: 10.3133/pp1862M.

Chen, W.-P. and Molnar, P. Focal depths of intracontinental and intraplate earthquakes and their implications for the thermal and mechanical properties of the lithosphere. *Journal of Geophysical Research: Solid Earth*, 88(B5):4183–4214, 1983. doi: 10.1029/JB088iB05p04183.

Chouet, B. A. Volcano seismology. *Pure and applied geophysics*, 160:739–788, 2003. doi: 10.1007/PL00012556.

Chouet, B. A. and Matoza, R. S. A multi-decadal view of seismic methods for detecting precursors of magma movement and eruption. *Journal of Volcanology and Geothermal Research*, 252:

108–175, 2013. doi: 10.1016/j.jvolgeores.2012.11.013.

Deichmann, N. Local magnitude, a moment revisited. *Bulletin of the Seismological Society of America*, 96(4A):1267–1277, 2006. doi: 10.1785/0120050115.

Gahlan, H. A., Azer, M. K., Asimow, P. D., and Al-Kahtany, K. M. Genesis and geodynamic evolution of serpentinized ultramafics and associated magnesite deposits in the Al-Wask ophiolite, Arabian Shield, Saudi Arabia. *American Journal of Science*, 320(3): 236–279, 2020. doi: 10.2475/03.2020.02.

Gudmundsson, A. Emplacement of dikes, sills and crustal magma chambers at divergent plate boundaries. *Tectonophysics*, 176 (3-4):257–275, 1990. doi: 10.1016/0040-1951(90)90073-H.

Hanks, T. C. and Kanamori, H. A moment magnitude scale. *Journal of Geophysical Research: Solid Earth*, 84(B5):2348–2350, 1979. doi: 10.1029/JB084iB05p02348.

Hill, D. P. A model for earthquake swarms. *Journal of Geophysical Research*, 82(8):1347–1352, 1977. doi: 10.1029/JB082i008p01347.

Hotovec-Ellis, A. J., Shelly, D. R., Hill, D. P., Pitt, A. M., Dawson, P. B., and Chouet, B. A. Deep fluid pathways beneath Mammoth Mountain, California, illuminated by migrating earthquake swarms. *Science advances*, 4(8):eaat5258, 2018. doi: 10.1126/sciadv.aat5258.

Johnson, P. R., Halverson, G. P., Kusky, T. M., Stern, R. J., and Pease, V. Volcanosedimentary basins in the Arabian-Nubian Shield: Markers of repeated exhumation and denudation in a Neoproterozoic accretionary orogen. *Geosciences*, 3(3):389–445, 2013. doi: 10.3390/geosciences3030389.

Klein, F. W. User's guide to HYPOINVERSE-2000, a Fortran program to solve for earthquake locations and magnitudes. Open-file Report 2002-171, US Geological Survey, 2002. doi: 10.3133/ofr02171.

Koulakov, I., El Khrepy, S., Al-Arifi, N., Sychev, I., and Kuznetsov, P. Evidence of magma activation beneath the Harrat Lunayyir basaltic field (Saudi Arabia) from attenuation tomography. *Solid Earth*, 5(2):873–882, 2014. doi: 10.5194/se-5-873-2014.

Koulakov, I., El Khrepy, S., Al-Arifi, N., Kuznetsov, P., and Kasatkina, E. Structural cause of a missed eruption in the Harrat Lunayyir basaltic field (Saudi Arabia) in 2009. *Geology*, 43(5):395–398, 2015. doi: 10.1130/G36271.1.

Molnar, P. The brittle-plastic transition, earthquakes, temperatures, and strain rates. *Journal of Geophysical Research: Solid Earth*, 125(7):e2019JB019335, 2020. doi: 10.1029/2019JB019335.

Monsalve, G., McGovern, P., and Sheehan, A. Mantle fault zones beneath the Himalayan collision: Flexure of the continental lithosphere. *Tectonophysics*, 477(1-2):66–76, 2009. doi: 10.1016/j.tecto.2008.12.014.

Ōmori, F. On the after-shocks of earthquakes. *Journal of the College of Science, Imperial University, Japan*, 7(2), 1894.

Pallister, J. S., McCausland, W. A., Jónsson, S., Lu, Z., Zahran, H. M., Hadidy, S. E., Aburukbah, A., Stewart, I. C., Lundgren, P. R., White, R. A., et al. Broad accommodation of rift-related extension recorded by dyke intrusion in Saudi Arabia. *Nature Geoscience*, 3(10):705–712, 2010. doi: 10.1038/ngeo966.

Pedregosa, F., Varoquaux, G., Gramfort, A., Michel, V., Thirion, B., Grisel, O., Blondel, M., Prettenhofer, P., Weiss, R., Dubourg, V., et al. Scikit-learn: Machine learning in Python. *Journal of machine Learning Research*, 12:2825–2830, 2011. https://www.jmlr.org/papers/volume12/pedregosa11a/pedregosa11a.pdf.

Prieto, G. A., Froment, B., Yu, C., Poli, P., and Abercrombie, R. Earthquake rupture below the brittle-ductile transition in continental lithospheric mantle. *Science Advances*, 3(3):e1602642, 2017. doi: 10.1126/sciadv.1602642.

Roberts, S. J., Husmeier, D., Rezek, I., and Penny, W. Bayesian approaches to Gaussian mixture modeling. *IEEE Transactions on Pattern Analysis and Machine Intelligence*, 20(11):1133–1142, 1998. doi: 10.1109/34.730550.

Ross, Z. E., Ben-Zion, Y., White, M. C., and Vernon, F. L. Analysis of earthquake body wave spectra for potency and magnitude values: Implications for magnitude scaling relations. *Geophysical Supplements to the Monthly Notices of the Royal Astronomical Society*, 207(2):1158–1164, 2016. doi: 10.1093/gji/ggw327.

Schulte-Pelkum, V., Monsalve, G., Sheehan, A. F., Shearer, P., Wu, F., and Rajaure, S. Mantle earthquakes in the Himalayan collision zone. *Geology*, 47(9):815–819, 2019. doi: 10.1016/j.epsl.2014.01.050.

Song, X. and Klemperer, S. L. Numerous Tibetan lower-crustal and upper-mantle earthquakes, detected by Sn/Lg ratios, suggest crustal delamination or drip tectonics. *Earth and Planetary Science Letters*, 626:118555, 2024. doi: 10.1016/j.epsl.2023.118555.

Stern, R. J. and Johnson, P. Continental lithosphere of the Arabian Plate: a geologic, petrologic, and geophysical synthesis. *Earth-Science Reviews*, 101(1-2):29–67, 2010. doi: 10.1016/j.earscirev.2010.01.002.

Tang, Z., Julià, J., Zahran, H., and Mai, P. M. The lithospheric shear-wave velocity structure of Saudi Arabia: young volcanism in an old shield. *Tectonophysics*, 680:8–27, 2016. doi: 10.1016/j.tecto.2016.05.004.

Utsu, T. A statistical study on the occurrence of aftershocks. *Geophys. Mag.*, 30:521–605, 1961. https://cir.nii.ac.jp/crid/1572261550806321280.

Wang, S. and Klemperer, S. L. Love-wave normal modes discriminate between upper-mantle and crustal earthquakes: Simulation and demonstration in Tibet. *Earth and Planetary Science Letters*, 571:117089, 2021. doi: 10.1016/j.epsl.2021.117089.

White, R. A. and McCausland, W. A. A process-based model of pre-eruption seismicity patterns and its use for eruption forecasting at dormant stratovolcanoes. *Journal of Volcanology and Geothermal Research*, 382:267–297, 2019. doi: 10.1016/j.jvolgeores.2019.03.004.

Wiemer, S. and McNutt, S. R. Variations in the frequency-magnitude distribution with depth in two volcanic areas: Mount St. Helens, Washington, and Mt. Spurr, Alaska. *Geophysical Research Letters*, 24(2):189–192, 1997. doi: 10.1029/96GL03779.

Woods, J., Winder, T., White, R. S., and Brandsdóttir, B. Evolution of a lateral dike intrusion revealed by relatively-relocated dike-induced earthquakes: The 2014–15 Bárðarbunga–Holuhraun rifting event, Iceland. *Earth and Planetary Science Letters*, 506: 53–63, 2019. doi: 10.1016/j.epsl.2018.10.032.

Xu, W., Jónsson, S., Corbi, F., and Rivalta, E. Graben formation and dike arrest during the 2009 Harrat Lunayyir dike intrusion in Saudi Arabia: Insights from InSAR, stress calculations and analog experiments. *Journal of Geophysical Research: Solid Earth*, 121(4):2837–2851, 2016. doi: 10.1002/2015JB012505.